BIOLOGICA NYSSANA
16 (1) June 2025: 267-276
DOI: 10.46793/BiolNyss.16.1.23A

Formulation and characterization of nanoparticles loaded with curcumin and amantadine as a promising neuroprotective agent

Original Article

Aksa Alex
Department of Pharmaceutics, Faculty of Pharmacy, Karpagam Academy of Higher Education, Coimbatore, Tamilnadu, India
Apsara Unni
Research Scholar, Department of Pharmaceutical Chemistry, JSS College of Pharmacy, Ooty, Tamilnadu, India
Gayathri Kumararaja
Department of Pharmaceutics, Faculty of Pharmacy, Karpagam Academy of Higher Education, Coimbatore, Tamilnadu, India
gayubpharm@gmail.com (corresponding author)

Received: *January 30, 2025*
Revised: *April 25, 2025*
Accepted: *April 28, 2025*

Abstract:

Parkinson's Disease (PD) is regarded as the second most common neurodegenerative disease and is characterized by observable motor dysfunction and loss of dopaminergic neurons. To date, there is no cure for PD, nor the treatment that stops its progression. Nanotechnology is very useful for controlling drug release, thus improving drug pharmacokinetic and pharmacodynamic properties. In this study, we fabricated curcumin- and amantadine-loaded nanoparticles using bovine serum albumin (BSA) as a nanocarrier using the desolvation method. Encapsulating curcumin and amantadine were beneficial in improving its aqueous solubility and bioavailability. The prepared nanoparticles had the particle size and zeta potential of 257 nm and -29 mV, respectively. The *in vitro* neuroprotective effect was determined using SHSY5Y cell lines through the MTT assay, which showed strong neuroprotective activity.

Key words:
bovine serum albumin, curcumin, amantadine, desolvation, neuroprotective activity

Apstrakt:

Formulisanje i karakterizacija nanočestica koje sadrže kurkumin i amantadin kao obećavajućeg neuroprotektivnog agensa

Parkinsonova bolest (PB) se smatra drugom najčešćom neurodegerativnom bolešću i karakteriše se izraženim motornim disfunkcijama i gubitkom dopaminergičkih neurona. Do danas ne postoji lek za PB, niti terapija koja može zaustaviti njeno napredovanje. Nanotehnologija se pokazala kao veoma korisna u kontroli oslobađanja lekova, čime se poboljšavaju farmakokinetička i farmakodinamička svojstva lekovitih supstanci. U ovoj studiji, metodom desolvatacije formirali smo nanočestice napunjene kurkuminom i amantadinom, koristeći albumin goveđeg seruma (BSA) kao nosač. Inkapsulacija kurkumina i amantadina doprinela je poboljšanju njihove rastvorljivosti u vodi i bioraspoloživost. Pripremljene nanočestice su imale veličinu čestica od 257 nm i zeta potencijal od -29 mV. *In vitro* neuroprotektivno dejstvo ispitano je na ćelijskim linijama SHSY5Y korišćenjem MTT testa, koji je pokazao izraženu neuroprotektivnu aktivnost.

Ključne reči:
albumin goveđeg seruma, kurkumin, amantadin, desolvatacija, neuroprotektivna aktivnost

Introduction

Parkinson's disease (PD) is a severe and debilitating neurodegenerative disorder that predominantly affects neurons in the brain. It is characterized by the progressive loss of dopaminergic neurons in the *substantia nigra pars compacta* (SNpc), leading to a deficiency of dopamine. Motor symptoms include bradykinesia, resting tremors, postural instability, and muscular rigidity. In addition to motor impairments, non-motor symptoms such as dementia, autonomic dysfunction, sleep disturbances, sensory abnormalities, depression, and anxiety are also frequently observed in patients (Poewe et al., 2017).

PD is the second most prevalent neurodegenerative disorder after Alzheimer's disease (AD), affecting approximately 35 to 100 individuals per 100,000 people globally (Simon et al., 2020). The worldwide prevalence of PD is estimated at 7 to 10 million individuals, with an average incidence of around

41 per 100,000 people. Notably, in populations aged 80 years and older, the prevalence increases significantly to 1,900 per 100,000 (Parkinson's News Today, 2021). Projections suggest that this number will rise to approximately 12.9 million by 2040 (Dorsey et al., 2018).

PD is a progressive and neurodegenerative disease first systematically described by James Parkinson, who referred to it as „shaking palsy" in his early observations (Parkinson, 2002). While Parkinson's terminology laid the groundwork, subsequent research has focused on understanding the clinical manifestations and slowing disease progression.

Since the degeneration of dopaminergic neurons cannot currently be halted or reversed, existing treatments for PD primarily aim to alleviate both motor and non-motor symptoms. A major limitation of current pharmacological therapies is their restricted ability to cross the blood-brain barrier (BBB), which limits central nervous system localization and often necessitates low-dose administrations (Tonda et al., 2018). Many treatments also suffer from issues such as low stability, potential toxicity of degradation by-products, high production costs, and limited neuroprotective efficacy—highlighting the need for further research.

Consequently, there is a pressing need for the development of novel drug delivery systems that can prolong and regulate drug release. Emerging trends in nanotechnology have demonstrated that nanoparticles (NPs) can enhance drug delivery by improving cellular uptake, reducing issues of low bioavailability, minimizing pharmacokinetic side effects, reducing the dosing frequency, and increasing drug concentration in targeted brain regions (Alonso et al., 2012; Yadav et al., 2025). Among these, controlled drug release systems are particularly promising due to their simplicity, reproducibility, and effectiveness. Nanotechnology-assisted delivery can significantly enhance both the pharmacokinetic and pharmacodynamic profiles of therapeutic agents.

Curcumin, a well-known polyphenolic compound with broad pharmacological activity (Gayathri et al., 2023), exhibits notable neuroprotective effects (Tsai et al., 2011; Nair et al., 2014). Its mechanisms of neuroprotection may include inhibition of reactive oxygen species (ROS) production due to its potent antioxidant and anti-inflammatory properties. Curcumin also affects glial cell function, α-synuclein aggregation, neuronal apoptosis, and ferroptosis. However, clinical application is limited by its poor oral bioavailability and low solubility (Young et al., 2014). These challenges may be mitigated through nano-based drug delivery systems (Takahashi et al., 2009; Cheng et al., 2013; Mourtas et al., 2014). Studies in *Drosophila* models of PD have shown that nanocurcumin significantly reduces PD symptoms, and it demonstrates higher bioavailability and neuroprotective activity in murine brains compared to conventional curcumin (Nazari et al., 2014).

Amantadine originally approved as an antiviral agent for influenza A (Staničová et al., 2001), has demonstrated antiviral activity against SARS-CoV-2 (Rascol et al., 2021) and anti-parkinsonian properties (Maksymiuk et al., 2021; Espay et al., 2024). It has also shown antiproliferative effects in various melanoma cell lines.

This study aims to develop and evaluate nanoparticles co-loaded with curcumin and amantadine for their neuroprotective potential in Parkinson's disease. The combination of curcumin and amantadine within a nanoparticle formulation may produce increased therapeutic effects, enhancing their individual benefits while reducing side effects. Improving BBB penetration and bioavailability through nanocarrier systems can help achieve sustained drug release, prolonged therapeutic action, and reduced dosing frequency.

Materials and Methods

Amantadine and curcumin were purchased from Yarrow Chem Products (Mumbai), bovine serum albumine (BSA) from Sigma, and ethanol and glutaraldehyde from Nice Chemicals Pvt Ltd (Kochi).

Preparation of albumin nanoparticles

Desolvation involves the addition of organic solvents to an aqueous solution of albumin, followed by chemical cross-linking with glutaraldehyde. The required amount of lyophilized BSA powder was dissolved in distilled water to make a BSA solution. The drug was dissolved in either ethanol or acetone separately. The pH was adjusted to between 7 and 8. A magnetic stirrer at 500 rpm was used for stirring until turbidity was observed by adding ethanol at a 1 mL/min rate. Glutaraldehyde was then added for cross-linking the BSA nanoparticles. Specifically, 0.1 mL of 4% glutaraldehyde solution was added, and the mixture was stirred for 2 hours. The stirring process was continued for 24 h, followed by five cycles of differential centrifugation (3000 rpm for 30 minutes), refining of the suspension, and resuspension of the pellet in a final volume of 10 mL distilled water. Finally, the nanoparticles were lyophilized and stored at 4 °C (Kim et al., 2010). A total of eight formulations (F1–F8) were prepared with varying concentrations of carrier and drug ratio.

Characterization

Drug-excipient compatibility studies (FTIR)

Compatibility between the drug and excipients used in the preparation of nanoparticles was confirmed by infrared spectroscopy. The nature of the interactions was identified. The samples were scanned using a Fourier Transform Infrared (FT-IR) spectrophotometer in the range of 4000 to 400 cm^{-1}. IR spectra of all individual drugs and synthesized nanoparticles were recorded. Furthermore, changes in appearance and peak positions were studied in the spectra to determine the possibility of chemical and physical interactions.

Particle shape and surface morphology

A scanning electron microscope (SEM; Zeiss EVO40) was used to examine the shape and morphology of the prepared nanoparticles. Samples were spread onto a slide using double-sided sticky tape, and the gold coating was done using a vacuum evaporator in an argon atmosphere assisted by gold flakes. Samples were scanned at various magnifications, and photomicrographs were captured.

Particle size and zeta potential

A concentrated solution of 1 mL albumin nanoparticles was diluted with 10 mL of water. The samples were analyzed using dynamic light scattering (DLS) with a Malvern Zetasizer. The polydispersity index (PDI) and average particle size were determined. Zeta potential was measured to assess formulation stability. The surface charge potential of the samples was analyzed in the Zetasizer chamber, and peaks were recorded to obtain zeta potential values. When interpreting the data, a monodisperse character is considered more desirable than a polydisperse one.

Drug entrapment efficiency

10 mL of the nanoparticle solution (equivalent to 10 mg of the drug) was transferred into a centrifuge tube. The mixture was centrifuged using a refrigerated centrifuge (Remi Motors, C-24 Plus) at 1000 rpm for 15 minutes at 25 °C. The supernatant was collected, and drug content was quantified using a calibration curve established by UV-visible spectrophotometry. Entrapment efficiency was calculated using the formula:

Encapsulation efficiency (%EE)=[(Total drug added–Free drug in supernatant)/Total drug added]×100

In vitro drug release study

The drug's release behavior from albumin nanoparticles was evaluated using the dialysis bag method. A predetermined volume of aqueous nanoparticle suspension was sealed in a dialysis bag and immersed in phosphate-buffered saline (PBS, pH 7.4) at 37 °C with stirring at 100 rpm. Samples were withdrawn from the release medium at specific intervals and replaced with fresh PBS. Samples were centrifuged, and the drug content in the supernatant was determined using HPLC or fluorescence/UV-visible spectrophotometry. A graph of cumulative drug release versus time was plotted.

Release kinetics study

In hydrophilic matrices, polymers swell and erode simultaneously, contributing to drug release. The resulting release profile often reflects zero-order kinetics. This study prepared a nanoformulation loaded with curcumin and amantadine for sustained release. The drug release data were fitted to various kinetic models: Zero-order (cumulative % drug released vs. time), First-order (log % drug remaining vs. time), Higuchi's model (cumulative % drug released vs. square root of time), and Korsmeyer–Peppas model (log % drug released vs. log time). The physicochemical properties, effectiveness, and quality of the nanoparticles were assessed using these models.

In vitro neuroprotective effect determination by MTT assay

SH-SY5Y (neuroblastoma) cell line was procured from the National Centre for Cell Sciences (NCCS), Pune, India, and maintained in Dulbecco's Modified Eagle's Medium (DMEM; Sigma Aldrich, USA). Cells were cultured in 25 cm^2 tissue culture flasks with DMEM supplemented with 10% fetal bovine serum (FBS), L-glutamine, sodium bicarbonate (Merck, Germany), and antibiotics: penicillin (100 U/mL), streptomycin (100 µg/mL), and amphotericin B (2.5 µg/mL). Cultures were maintained at 37 °C in a humidified 5% CO_2 incubator (NBS Eppendorf, Germany). Cell viability was assessed by inverted phase-contrast microscopy and further confirmed via MTT assay.

Cytotoxicity evaluation

Once cells reached sufficient growth, rotenone (10 µM) was added to induce cytotoxicity and incubated for 1 hour. After incubation, the medium was removed, and freshly prepared compounds were added in concentrations of 25, 12.5, 6.25, 3.1, and 1.5 µg/mL. Each concentration was added in triplicate to the respective wells. Control and rotenone-only wells were maintained for comparison.

Microscopic observation

After 24 hours of treatment, plates were observed

under an inverted phase contrast microscope (Olympus CKX41 with Optika Pro5 CCD camera). Morphological changes such as cell rounding, shrinkage, granulation, and vacuolization were noted as indicators of cytotoxicity.

MTT assay

Fifteen mg of MTT (Sigma, M-5655) was reconstituted in 3 mL PBS and sterilized by filtration. After 24 hours of incubation, 30 µL of MTT solution was added to each well and incubated for 4 hours at 37 °C in a humidified 5% CO_2 incubator. After incubation, the supernatant was removed, and 100 µL of DMSO (Sigma Aldrich, USA) was added to dissolve the formazan crystals. Absorbance was read using a microplate reader at 540 nm (Talarico et al., 2004).

The percentage of growth inhibition was calculated using the formula:

% of viability = (Mean OD Samples x 100)/ Mean OD of control group

Results and discussion

Particle size, PDI, and zeta potential

The particle size and PDI of the nanoparticles were measured using the DLS technique and a computerized zetasizer. A Zetasizer cell was loaded with nanoformulation, and the measurements were taken. Values of all particle sizes in the different formulations (**Tab. 1**) were at the nanometer scale. Particle size, zeta potential, and PDI for formulation F7 (**Fig. 1a**, **Fig. 1b**) were 257.8 nm, -29 mV, and 0.05, respectively. The size of the nanoparticles was 255.5 nm to facilitate uptake into the cell and delivery to the appropriate site. Another important characteristic parameter of nanoparticles is PDI. For example, a PDI below 0.05 shows that the population is very monodisperse, and a PDI of greater than 0.7

Table 1. Particle size, zeta potential and PDI values of optimized nanoformulation

Formulation code	Particle size (nm)	Zeta Potential (mv)	PDI
F1	1349	-12.6	0.13
F2	857.5	-21.4	0.71
F3	906.4	-17.7	0.62
F4	589.1	-11.5	0.91
F5	496.8	-21.6	0.47
F6	272.4	-28.4	0.32
F7	255.5	-29.1	0.05
F8	257.8	-21.4	0.52

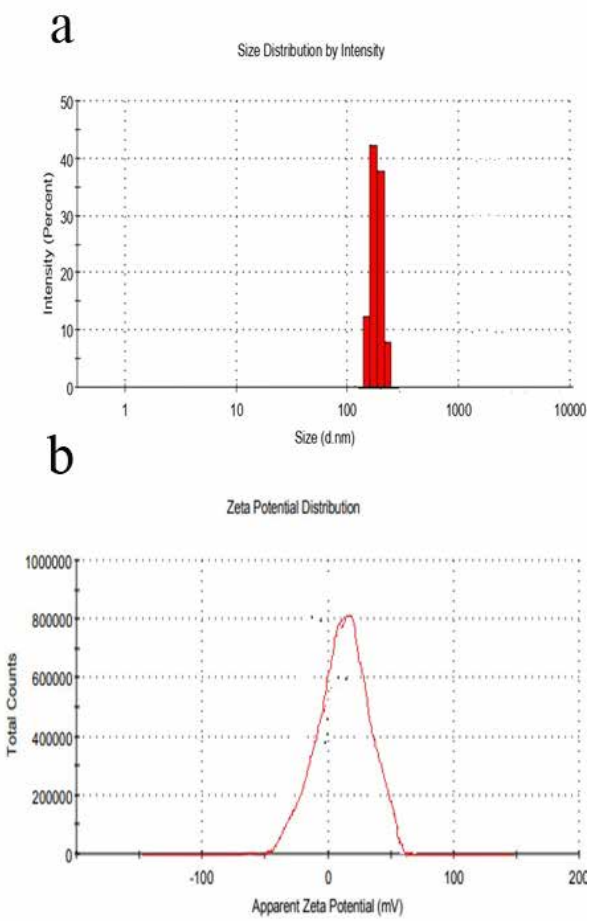

Fig. 1. Particle size distribution graph and zeta potential distribution graph of F7 formulation

means the size distribution is wide. The result of this experiment also indicated a PDI of 0.05, signifying no significant variation in particle sizes, along with a zeta potential of -29 mV that is adequate electrostatic repulsion, stabilizing the suspension and preventing agglomeration of the particles.

Although the particle size of 257.8 nm may seem relatively large, it falls within the optimal range (100–300 nm) for effective brain-targeted delivery. Such sizes are known to cross the blood-brain barrier via transcytosis mechanisms. Additionally, the narrow PDI (0.05) and stable zeta potential (–29 mV) indicate a uniform and stable formulation. Larger nanoparticles in this range can also offer advantages such as higher drug-loading capacity and sustained release, which are beneficial for neuroprotective applications.

Entrapment efficiency

The entrapment efficiency of the formulation is based on the properties of the polymer, drug, and desolvating agent. The prepared nanoparticles were investigated using a refrigerated centrifuge method to determine this parameter. The nanoparticles

were centrifuged at 3000 rpm for 30 minutes. The supernatant, containing the un-entrapped drug, was collected and quantified using a UV spectrophotometer at a wavelength of 425 nm (**Fig. 2**). The entrapment efficiency across all batches varied between 45.61% and 72.92%, with formulation F7 showing the highest efficiency. The high entrapment efficiency of 72.92% indicates significant drug loading, suggesting that this formulation has excellent potential for achieving a good therapeutic payload. High concentrations of polymer and ethanol enhanced the entrapment efficiency, as the drug is lipophilic. The increased lipid content improved the solubilization of the lipophilic drug, creating additional space within the matrix for drug entrapment.

In vitro release study

The *in vitro* drug release profile of the formulations is shown graphically. The drug release profiles indicate different release rates over a period of 8 hours. In the formulations, F1 to F5 showed relatively higher cumulative drug release percentages, and around 40–45% were released at the end of the study. Formulations F6, F7, and F8 show slow release, but F7 showed a prolonged drug release profile, with the lowest cumulative drug release among all the formulations. The formulation composition of F7 would be responsible for the sustained release behavior due to its possible enhancement of drug encapsulation and minimization of rapid diffusion (**Fig. 3**). Such characteristics are advantageous for controlled drug delivery systems in ensuring prolonged therapeutic effects and reducing the number of administrations. This highlights the significant role of formulation variables in adjusting the release kinetics to meet the therapeutic requirements.

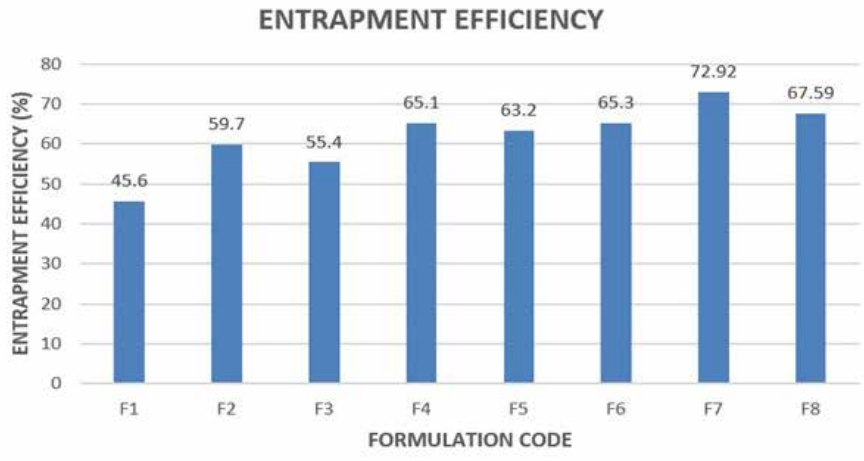

Fig. 2. Entrapment efficiency graph of nanoformulations

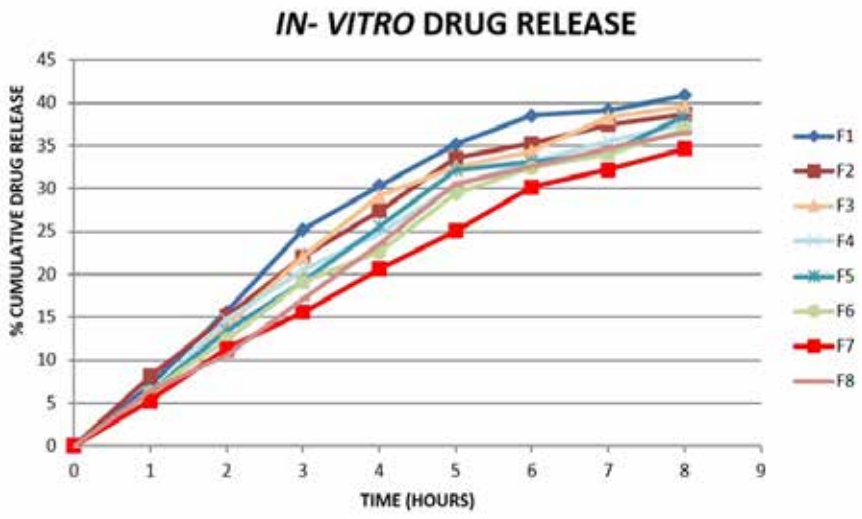

Fig. 3. *In vitro* drug release graph of F1 to F8 nanoformulation

Release kinetics study

The drug release is in zero-order kinetics since the R^2 of 0.917 shows that it is constant with time and does not depend on the drug concentration within the nanoparticles; this behavior displays the system's controlled-release properties, such that it offers predictable, consistent drug release and, hence, sustainable therapeutic levels for an extensive period.

This suggests that the mechanism is diffusion-controlled and further indicates that the diffusion in the nanoparticle matrix controls the release rate of the drug rather than any other controlling mechanism. The R^2 value of 0.9245 for the Higuchi model further confirms this since the drug release varies as a square root function of time.

The Korsmeyer–Peppas model with an R^2 of 0.9735 shows a non-Fickian or anomalous release mechanism, meaning that drug release that is subjected to diffusion within the polymeric matrix, along with the relaxation of polymer chains, will depict such a mechanism (**Tab. 2**,

Table 2. Release kinetics of F7 Formulation

Model name	Zero order kinetics	First order kinetics	Higuchi model	Korsmeyer peppas model
R^2 value	0.917	0.8512	0.9245	0.9735

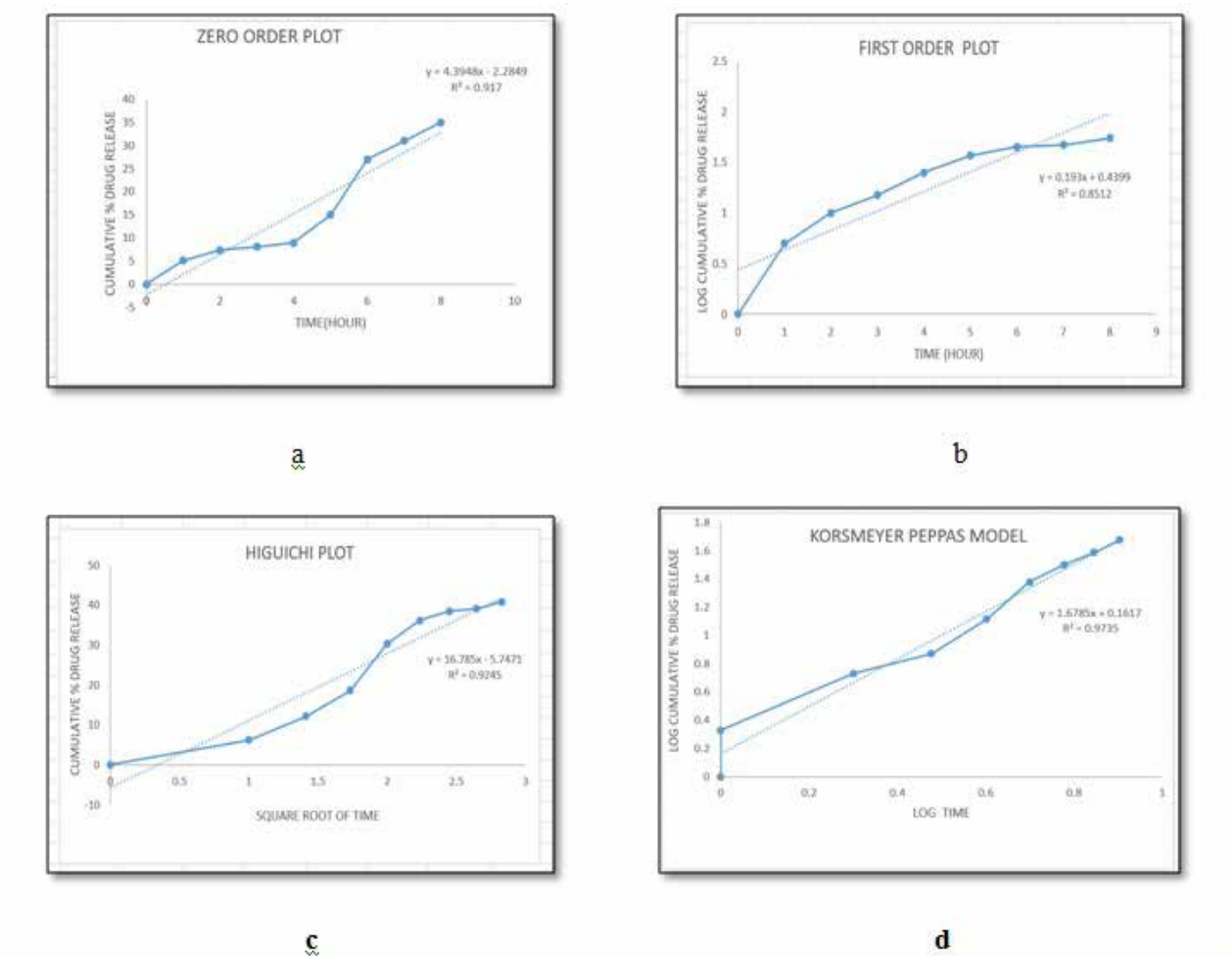

Fig. 4. Release kinetics of F7 Formulation (**a** - zero order kinetics; **b** - first order kinetics; **c** - Higuchi plot; **d** - Korsmeyer Peppas plot)

Fig. 4). Thus, it exemplifies an interplay between diffusion-driven and matrix relaxation-controlled processes, thereby offering more complex, reliable drug delivery systems targeted for sustained therapeutic outcomes.

In vitro neuroprotective effect determination by MTT assay

The neuroprotective potential of the sample combination (curcumin+amantadine) was assayed by carrying out the MTT assay with the neurotoxic agent rotenone. Rotenone was selected as the neurotoxic agent in this study due to its well-established ability to mimic Parkinson's disease by inducing oxidative stress and dopaminergic neuron damage through mitochondrial complex I inhibition in *in vitro* and *in vivo* models. Hence, it is an appropriate choice for modeling PD-related neurotoxicity.

Cells without treatment were kept aside to control. OD values for the diverse concentrations of samples within 1.5 to 25 µg/mL are obtained, and respective percentages of cell viability are calculated. The control group had the highest average OD value, 0.8725, which means 100% cell survival. However, rotenone-treated cells displayed a drastic reduction in viability, and the average OD value was 0.4179, which translated to 47.90%. This confirms the potent neurotoxic effect of rotenone.

The curcumin+amantadine formulation increased the cell viability in a concentration-dependent manner. The sample with the lowest concentration of 1.5 µg/mL had an average OD of 0.4703 and a

cell viability of 53.90%. A slight recovery from rotenone-induced cytotoxicity was noted. With the increase to 3.1 µg/mL, the average OD became 0.5484, and cell viability reached 62.85%, meaning that the protective effect is moderate.

The average OD at 6.25 µg/mL increased further to 0.6011, corresponding to 68.90% cell viability. This trend continued well up to 12.5 µg/mL, where at that concentration, the average OD reached 0.6591, with the equivalence of 75.54% viability. The maximal protective effect was obtained with an average OD of 0.7301 and 83.68% cell viability, with the highest concentration tested being at 25 µg/mL (**Tab. 3**).

(OD), percentage viability, standard deviations (Stdev), and standard error (SE). The statistics that accompanied the experiment verified the results and validated the effectiveness of the sample with various concentrations.

The control received no treatment, and cell viability remained 100% at all the time points, with an average OD of 0.8725, showing no variability (Stdev=0, SE=0). Results will form the comparison control. The results from cytotoxicity for the samples that were treated with rotenone showed a very high statistical significance for the remaining average percentage of cell viability at about 47.91% as opposed to the control average. This would mean

Table 3. OD Values of curcumin+amantadine nanoparticles

Sample concentration(µg/mL)	OD value I	OD value II	OD value III	Average OD	Percentage viability
Control	0.8748	0.8817	0.8609	0.8725	100
Rotenone	0.4208	0.4131	0.4198	0.4179	47.9
Sample code: Curcumin + Amantadine					
1.5	0.4643	0.4729	0.4737	0.4703	53.9
3.1	0.5514	0.5413	0.5525	0.5484	62.85
6.25	0.5956	0.6068	0.601	0.6011	68.9
12.5	0.656	0.6639	0.6574	0.6591	75.54
25	0.7324	0.7229	0.7351	0.7301	83.68

These results indicate that curcumin and amantadine formulations indeed possess a good neuroprotective potential as they rescue rotenone-induced cytotoxicity in a concentration-dependent manner. The progressive increase in percentage viability as concentration increases implies that the formulation could perhaps neutralize oxidative stress and neuronal damages, probably due to the synergism of curcumin through antioxidant properties and amantadine's neuroprotective mechanisms. The potential of this combination of therapies can be a bright prospect as a therapeutic measure for oxidative stress-related and neuronal damage-related neurodegenerative conditions. The findings suggest significant neuroprotective effects of the drug from an increase in percentage viability and betterment of cell morphology.

Statistical analysis of in vitro neuroprotective effect using MTT assay

The neuroprotective activity of the curcumin+amantadine combination was investigated on the SH-SY5Y cell line. Data were obtained from the MTT assay, which used optical density

that neurotoxicity would have a significantly high degree. The two variables, Stdev=0.97015 and SE=0.32338 illustrate the variation in the cytotoxic-induced response (**Tab. 4**).

In this study, the curcumin+amantadine treatment demonstrated a concentration-dependent effect on cell viability improvement. On 1.5 µg/mL, the mean percentage viability was 53.91% (Stdev=1.00335, SE=0.33445), representing partial protection from rotenone-induced damage. Successively higher concentrations showed increasingly increased percent viability, such as up to 3.70% at 25 µg/mL (Stdev=1.69913, SE=0.56638). This significant recovery reveals a synergistic action between curcumin and amantadine against neuronal damage.

The trend for cell viability at a higher concentration of curcumin+amantadine was statistically analyzed to determine the decreasing variability at intermediate concentrations: 6.25 µg/mL, Stdev=0.86632, SE=0.28877; thus, there may be uniform protection at such doses. The highest dose, 25 µg/mL, yielded the highest variability at Stdev=1.69913, possibly because the high dose of the sample triggered an increase in metabolic

Table 4. Percentage viability of curcumin+amantadine nanoparticles

Cell Line SHSY-5Y									
SAMPLE CODE-Curcumin + Amantadine	OD1	OD2	OD3	Percentage Viability 1	Percentage Viability 2	Percentage Viability 3	Average	Std Dev	Std Error
Control	0.8748	0.8817	0.8609	100	100	100	100	0	0
Rotenone	0.4208	0.4131	0.4198	48.1024	46.8527	48.7629	47.906	0.97015	0.32338
1.5	0.4643	0.4729	0.4737	53.075	53.635	55.0238	53.9113	1.00335	0.33445
3.1	0.5514	0.5413	0.5525	63.0316	61.3928	64.177	62.8671	1.39939	0.46646
6.25	0.5956	0.6068	0.601	68.0841	68.8216	69.8107	68.9055	0.86632	0.28877
12.5	0.656	0.6639	0.6574	74.9886	75.2977	76.3619	75.5494	0.72045	0.24015
25	0.7324	0.7229	0.7351	83.722	81.9893	85.3874	83.6996	1.69913	0.56638

activity and/or variability in cellular response.

The bar graph represents the neuroprotective action (**Fig. 5**). Control and rotenone-treated samples are two extremes wherein the viability was highly different. The bars related to curcumin-amantadine-treated samples represent a considerable positive trend in the recovery process, indicating that the increase is concentration-dependent. The error bars depict that at middle concentrations (6.25–12.5 µg/mL), the values are more accurate.

Statistical analysis confirms that the neuroprotective effects of the combination of curcumin and amantadine are indeed dose-dependent. Percent viabilities are high regarding protection against cytotoxicity from rotenone at concentrations of 12.5–25 µg/mL; data approach near-control levels. The consistency and reproducibility of these data at key concentrations, evidenced by low standard errors, support the therapeutic potential for this combination (**Fig. 6a-6f**). These results support further exploration of curcumin and amantadine as a synergistic neuroprotective strategy in oxidative stress and neurodegeneration models.

Conclusion

In this study, we fabricated curcumin and amantadine nanoparticles using bovine serum albumin (BSA) as a nanocarrier using the desolvation method for antiparkinson activity. Eight nanoformulations were prepared by varying the concentration of ethanol, glutaraldehyde, and stirring time. The nanoparticles were acquired in the particle size of 255.5 nm, within the optimal range for cellular growth and targeted delivery. PDI was found to be 0.05, indicating a highly uniform size distribution, and a zeta potential of -29 mV is generally considerably stable, indicating a sufficient electrostatic repulsion between particles to prevent aggregation. Nanoparticles showed a sustained release profile, and both diffusion and relaxation-controlled processes influence the mechanism of drug release. The results of *in vitro* antiparkinson activity confirmed that the optimized nanoparticle has significant neuroprotective effects of the drug from an increase in percentage viability and betterment of cell morphology. Hence, a combination of curcumin and amantadine nanoparticles will be a better choice for neuroprotective effects.

Acknowledgements. I would like to thank the Centre for Food Nanotechnology, Karpagam Academy of Higher Education, Coimbatore for helping me to perform particle size analysis and zeta potential characterization.

References

Alonso, M.J. & Couvreur, P. (2012). Historical view

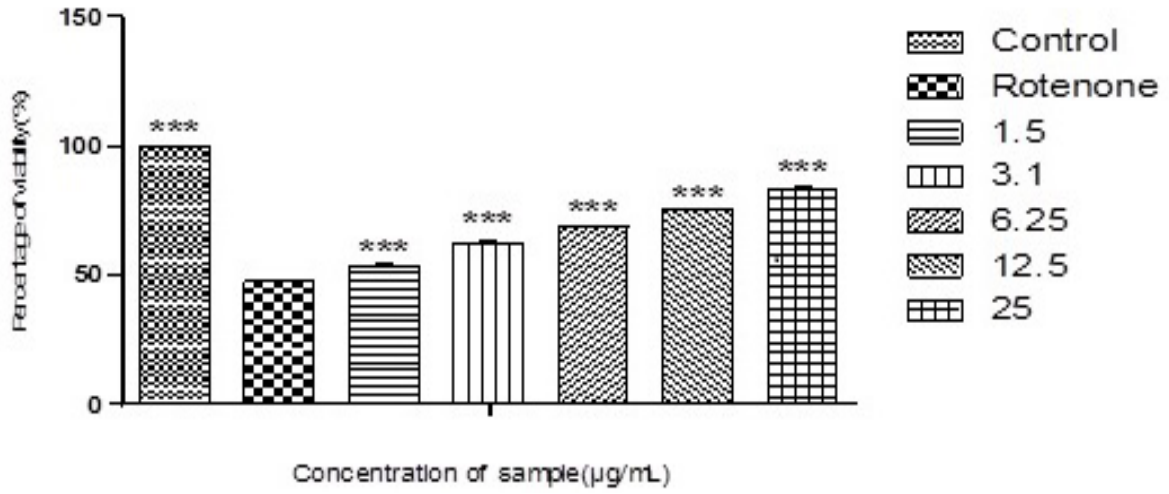

Fig. 5. Percentage viability of cells

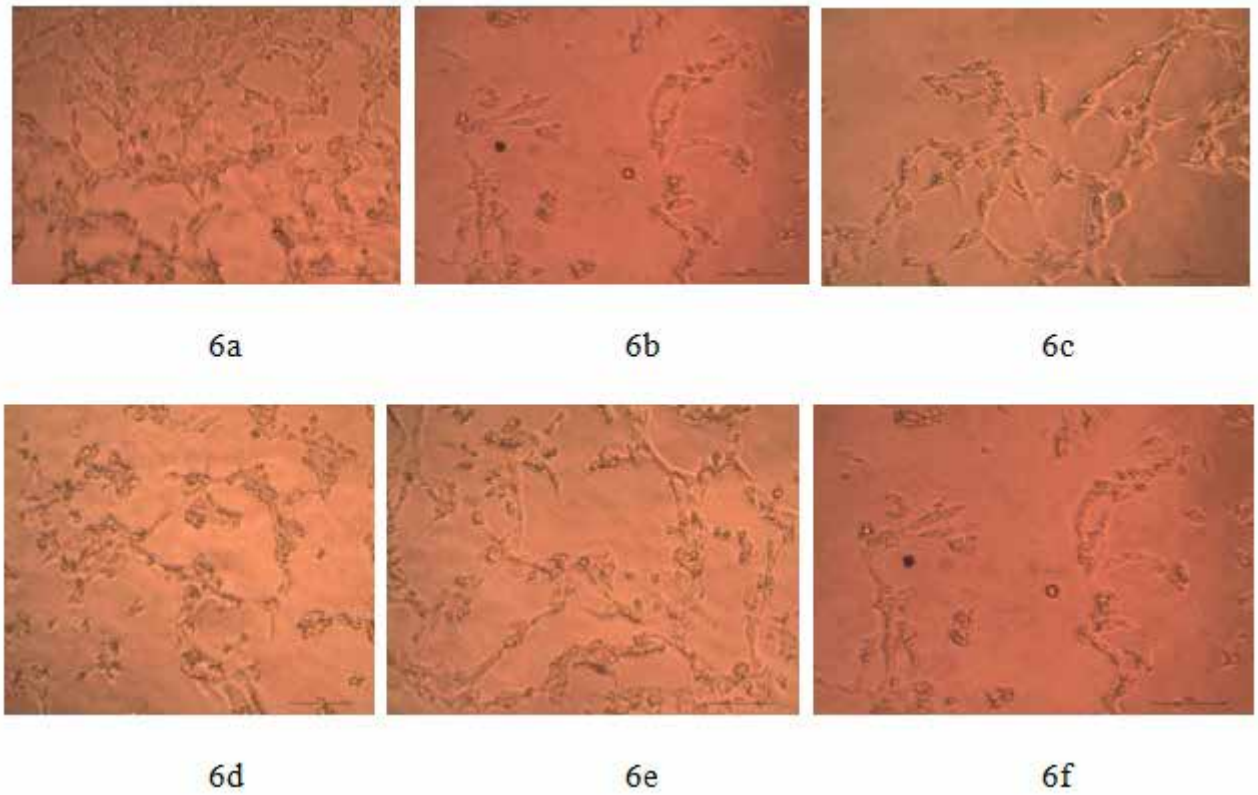

Fig. 6. Microscopic images of control (**6a**), rotenone (**6b**), varied concentrations of nanoparticle 1.5 µg/mL (**6c**), 3.1 µg/mL (**6d**), 6.25 µg/mL (**6e**), and 12.5 µg/mL (**6e**)

of the design and development of nanocarriers for overcoming biological barriers. In: *Nanostructured Biomaterials for Overcoming Biological Barriers* (pp. 3-36). UK, Cambridge: The Royal Society of Chemistry.

Cheng, K.K., Yeung, C.F., Ho, S.W., Chow, S.F., Chow, A.H., & Baum, L. (2013). Highly stabilized curcumin nanoparticles tested in an *in vitro* blood–brain barrier model and in Alzheimer's disease Tg2576 mice. *The AAPS journal*, *15*, 324-336. doi: 10.1208/s12248-012-9444-4.

Dorsey, E.R. & Bloem, B.R. (2018). The Parkinson pandemic - a call to action. *JAMA neurology*, *75*(1), 9-10. doi: 10.1001/jamaneurol.2017.3299.

Espay, A.J., Ostrem, J.L., Formella, A.E., & Tanner, C.M. (2024). Extended-release amantadine for OFF-related dystonia in Parkinson's disease. *Parkinsonism & Related Disorders*, *122*, 106088.

https://doi.org/10.1016/j.parkreldis.2024.106088

Fink, K., Nitsche, A., Neumann, M., Grossegesse, M., Eisele, K.H., & Danysz, W. (2021). Amantadine inhibits SARS-CoV-2 *in vitro*. *Viruses*, *13*(4), 539.

Kim, T.H., Jiang, H.H., Youn, Y.S., Park, C.W., Tak, K.K., Lee, S., Kim, H., Jon, S., Chen, X., & Lee, K.C. (2011). Preparation and characterization of water-soluble albumin-bound curcumin nanoparticles with improved antitumor activity. *International Journal of Pharmaceutics*, *403*(1-2), 285-291. doi: 10.1016/j.ijpharm.2010.10.041.

Gayathri, K., Bhaskaran, M., Selvam, C., & Thilagavathi, R. (2023). Nano formulation approaches for curcumin delivery-a review. *Journal of Drug Delivery Science and Technology*, *82*, 104326. https://doi.org/10.1016/j.jddst.2023.104326.

Maksymiuk, A.W., Tappia, P.S., Bux, R.A., Moyer, D., Huang, G., Joubert, P., Miller, D.W., Ramjiawan, B., & Sitar, D.S. (2021). Use of amantadine in the evaluation of response to chemotherapy in lung cancer: A pilot study. *Future Science OA*, *7*(4), FSO679. doi: 10.2144/fsoa-2020-0176.

Mourtas, S., Lazar, A.N., Markoutsa, E., Duyckaerts, C., & Antimisiaris, S.G. (2014). Multifunctional nanoliposomes with curcumin–lipid derivative and brain targeting functionality with potential applications for Alzheimer disease. *European Journal of Medicinal Chemistry*, *80*, 175-183. doi: 10.1016/j.ejmech.2014.04.050.

Nair, P., Malhotra, A., & Dhawan, D.K. (2015). Curcumin and quercetin trigger apoptosis during benzo(a)pyrene-induced lung carcinogenesis. *Molecular and Cellular Biochemistry*, *400*, 51-56. doi: 10.1007/s11010-014-2261-6.

Nazari, Q.A., Takada-Takatori, Y., Hashimoto, T., Imaizumi, A., Izumi, Y., Akaike, A., & Kume, T. (2014). Potential protective effect of highly bioavailable curcumin on an oxidative stress model induced by microinjection of sodium nitroprusside in mice brain. *Food & Function*, *5*(5), 984-989. doi: 10.1039/c4fo00009a.

Parkinson, J. (2002). An essay on the shaking palsy. *The Journal of neuropsychiatry and clinical neurosciences*, *14*(2), 223-236. doi: 10.1176/jnp.14.2.223.

Parkinson's News Today (2021). *Parkinson's Disease Statistics*. Retrieved from https://parkinsonsnewstoday.com/parkinsons-disease-statistics (accessed on 8 December 2021).

Poewe, W., Seppi, K., Tanner, C.M., Halliday, G.M., Brundin, P., Volkmann, J., Schrag, A.E., & Lang, A.E. (2017). Parkinson disease. *Nature reviews Disease Primers*, *3*(1), 1-21. https://doi.org/10.1038/nrdp.2017.13

Rascol, O., Fabbri, M., & Poewe, W. (2021). Amantadine in the treatment of Parkinson's disease and other movement disorders. *The Lancet Neurology*, *20*(12), 1048-1056. doi: 10.1016/S1474-4422(21)00249-0.

Simon, D.K., Tanner, C.M., & Brundin, P. (2020). Parkinson disease epidemiology, pathology, genetics, and pathophysiology. *Clinics in Geriatric Medicine*, *36*(1), 1-12. doi: 10.1016/j.cger.2019.08.002.

Staničová, J., Miškovský, P., & Šutiak, V. (2001). Amantadine: an antiviral and antiparkinsonian agent. *Veterinární medicína, Czech Academy of Agricultural Sciences*, *46*(9), 244-256.

Takahashi, M., Uechi, S., Takara, K., Asikin, Y., & Wada, K. (2009). Evaluation of an oral carrier system in rats: bioavailability and antioxidant properties of liposome-encapsulated curcumin. *Journal of Agricultural and Food Chemistry*, *57*(19), 9141-9146. doi: 10.1021/jf9013923.

Tonda-Turo, C., Origlia, N., Mattu, C., Accorroni, A., & Chiono, V. (2018). Current limitations in the treatment of Parkinson's and Alzheimer's diseases: state-of-the-art and future perspective of polymeric carriers. *Current Medicinal Chemistry*, *25*(41), 5755-5771. doi: 10.2174/0929867325666180221125759.

Tsai, Y.M., Chien, C.F., Lin, L.C., & Tsai, T.H. (2011). Curcumin and its nanoformulation: the kinetics of tissue distribution and blood–brain barrier penetration. *International Journal of Pharmaceutics*, *416*(1), 331-338. doi: 10.1016/j.ijpharm.2011.06.030.

Yadav, V.K., Dhanasekaran, S., Choudhary, N., Nathiya, D., Thakur, V., Gupta, R., Pramanik, S., Kumar, P., Gupta, N., & Patel, A. (2025). Recent advances in nanotechnology for Parkinson's disease: diagnosis, treatment, and future perspectives. *Frontiers in Medicine*, *12*, 1535682. doi:10.3389/fmed.2025.1535682.

Young, N.A., Bruss, M.S., Gardner, M., Willis, W.L., Mo, X., Valiente, G.R., Cao, Y., Liu, Z., Jarjour, W.N., & Wu, L.C. (2014). Oral administration of nano-emulsion curcumin in mice suppresses inflammatory-induced NFκB signaling and macrophage migration. *PloS One*, *9*(11), e111559. doi: 10.1371/journal.pone.0111559.